



OPEN

Multi-band circularly polarized patch antenna with CPW feed based on sunflower geometry and Gielis superformula for wireless communication

Kanika Joshi¹, Gaurav Kumar Soni² & Dinesh Yadav²✉

In modern wireless communication systems, antennas that support multiple wireless standards, enabling applications such as WLAN, Wi-Fi, WiMAX, C-band, RFID and 5G NR are essential. These multi-band antennas help reduce both system space and cost. This paper presents a multi-frequency broadband circularly polarized patch antenna based on Gielis's superformula. The multiband characteristics are achieved through a sunflower-inspired multi-ringed patch structure. The antenna is designed on a 59.691 mm × 60.41 mm Rogers RO4003 substrate and utilizes a CPW feed, which enhances the bandwidth from 0.88 to 1.61 GHz (L-band), 2.46–2.60 GHz (S-band), and 4.87–6.49 GHz (C-band). Circular polarization in the C-band is achieved by introducing slots in the ground plane. The proposed design demonstrates operation at central frequencies of 1.06 GHz, 2.56 GHz, and 5.8 GHz. Simulated and measured results of return loss, radiation patterns, and realized gain show good agreement.

Keywords Multi-Band, Gielis superformula, CPW feed, Sunflower geometry, Circularly polarized

Circularly polarized antennas are becoming a natural choice of wireless communications technologies like satellite communication, radars, and global positioning systems, etc. for their advantage to reduce multipath effect and irrelevance of antenna orientation^{1,2}. Various types of circularly polarized antenna such as helix antenna, spiral antenna, dielectric resonator microstrip patch antenna, etc. have been investigated during the past few decades^{3,4}. Among them, circularly polarized microstrip patch antennas have attracted significant research interest due to their advantages of low cost, low profile, and ease of fabrication, despite limitations such as narrow bandwidth and low gain performance¹. Several techniques, such as the use of various geometries, different types of slots, and mathematical approaches like Fourier analysis and super-ellipse equations, have been applied to improve bandwidth^{5,6}.

One such technique involves the use of natural forms or shapes generated using the superformula, developed by Gielis and reported in⁷. The fundamental basis for the equation is of a circle in which the mathematician Gabriel Lamé generalized ellipse equation is inserted where the power of 2 is replaced with any real number n and the equation is scaled along X and Y axis.

$$\frac{x}{a}^n + \frac{y}{b}^n = 1 \quad (1)$$

Gielis's breakthrough was to expand the superellipse concept to polar coordinates, enabling a much wider range of shapes to be described. In polar coordinates, the superformula is represented as

¹Department of Electronics and Communication Engineering, Parmanand Sharma Smriti Mahavidyalaya, Jodhpur, India. ²Department of Electronics and Communication Engineering, Manipal University Jaipur, Jaipur, Rajasthan, India. ✉email: dinesh.yadav@jaipur.manipal.edu

$$r = \left(\left| \frac{\cos \frac{m\theta}{4}}{a} \right|^{n_2} + \left| \frac{\sin \frac{m\theta}{4}}{b} \right|^{n_3} \right)^{\frac{1}{n_1}} \quad (2)$$

Where, the number of ends is decided by the value of m. The value of a and b decides the symmetry of the design and n_1 , n_2 and n_3 are used to determine the position of the ends.

This mathematical formula is used to design various 2D natural or artificial shapes. The resulting designs are more precise and proportionate, as the formula accounts for the number of edges and indentations in the shape. Experimental research in this area has introduced a new class of patch geometries for various microwave applications. For example, A. Omar et al. proposed an ultra-wideband circular patch antenna with a sawtooth-like circumference, as discussed in⁶. The antenna operates over a 3.1–10.6 GHz bandwidth but exhibits linear polarization with no frequency notches. The same group later proposed a modified design, described in⁸, incorporating two arc-shaped slots and one split-ring resonator (SRR) in the ground plane, which generates two frequency notches at the WiMAX and WLAN bands while maintaining linear polarization.

Mao et al. proposed a wideband dual-sense circularly polarized (CP) helical array antenna with enhanced isolation. The design utilizes two concentric helical antennas with opposite winding directions and different radii to achieve left-handed (LHCP) and right-handed (RHCP) CP radiation within the same frequency band. A 2×2 array configuration with sequentially rotated microstrip feeding networks on the same plane was implemented to further enhance performance. The fabricated prototype achieved overlapping impedance and 3 dB axial ratio (AR) bandwidth from 3.7 GHz to 5.0 GHz (30% fractional bandwidth), with isolation better than 22 dB, demonstrating excellent dual-polarization characteristics⁹. Chen et al. proposed a bandwidth-enhanced full-metal circularly polarized cavity-backed slot antenna and array using two pairs of degenerate modes within a single cavity. Unlike conventional CP antennas with a single AR minimum, their design achieves two AR minima, resulting in wider bandwidth. Metal prisms are introduced to bring the two CP bands closer together, enhancing the operational bandwidth. A 2×2 cross-slot array, directly fed by cavity modes, eliminates the need for additional power dividers. The fabricated antenna achieved a 15% bandwidth, a peak gain of 11.8 dBic, and a total efficiency of 96%¹⁰. Naser et al. designed a compact ultrawideband (UWB) MIMO antenna by placing two single-pole super-formula-based antenna elements at 180° orientation. The results demonstrated low envelope correlation coefficient (ECC) and good group delay performance, indicating favorable diversity characteristics¹¹. Poordaraee et al. proposed an eye-drop-shaped patch antenna with an elliptical cut, achieving circular polarization at 2.45 GHz. The design is a single-band, narrow-band, circularly polarized patch antenna with a low return loss coefficient¹². Bhaskar et al. introduced a CPW-fed antenna utilizing a super-shaped slot and super-shaped patch. The simulated results exhibited UWB performance from 2.5 GHz to approximately 9 GHz with an almost constant gain of around 5 dB¹³. Sun et al. proposed an ultrawideband circularly polarized halved-type Vivaldi antenna (HVA) with symmetrical radiation patterns. The design features a rotational-symmetry structure where each HVA element serves as both the radiator and ground plane, eliminating the need for an additional ground plane. A compact sequential phase feeding network is integrated into the design. The fabricated antenna achieved an impedance bandwidth of 111.5% (0.52–1.83 GHz), a 3 dB axial ratio bandwidth of 100% (0.49–1.47 GHz), and a peak gain of 7.2 dBic². Wei et al. proposed a dual-band rotational-feed circularly polarized antenna array using two pairs of symmetric dipoles. The low-frequency CP radiation is achieved by longer dipoles, while the high-frequency CP radiation results from the combination of shorter dipoles and higher-order modes. A compact 1-to-4 rotational feeding network was employed. The antenna achieved $|S_{11}| < -10$ dB from 0.8 to 1.26 GHz and 2.15–2.82 GHz, with 36.3% AR bandwidth at low frequency and 24.5% at high frequency. The realized gains were 7.7 dBic and 12.3 dBic, with symmetric radiation patterns¹⁴. An et al. proposed a dual-band, dual-sense circularly polarized antenna using a microstrip-line-fed, slot-coupled magneto-electric dipole (ME-dipole) structure. In this design, the coupling slot serves both as a feeding structure and a radiating element, enabling LHCP and RHCP generation without the need for two separate antennas. The design achieved dual-band impedance bandwidths of 18.2% (2.14–2.57 GHz) and 17.8% (3.78–4.52 GHz), with LHCP and RHCP axial ratio bandwidths of 21.3% and 25.9%, respectively¹⁵. Fathima et al. proposed a compact fractal Koch-shaped slot antenna achieving seven resonant bands (1.7–6.7 GHz) with impedance bandwidths of 1.6%–9.8%, suitable for GPS, WLAN, WiMAX, and satellite applications¹⁶. Goel et al. designed a single-layer, proximity-fed circularly polarized antenna with orthogonal circular slots, covering dual bands (3.2–3.9 GHz and 4.9–5.6 GHz) and compact size ($80 \times 80 \times 1.6$ mm³)¹⁷. Ali et al. introduced a compact patch antenna for WBAN at 2.4 GHz ISM band with high efficiency (53% off-body, 46% on-body), low SAR, and stable far-field patterns ($62 \times 43 \times 1.67$ mm³)¹⁸. An et al. developed a dual-band dual-sense CP antenna using a slot-coupled ME-dipole, achieving wide AR bandwidths of 21.3% and 25.9% at 2.14–2.57 GHz and 3.78–4.52 GHz, respectively¹⁵.

In this paper, a multi-frequency broadband circularly polarized patch antenna based on Gielis's superformula is presented. The antenna is fed using a coplanar waveguide (CPW) feed. The feed consists of a central conducting strip and two ground planes placed around it, printed on the same side of the dielectric substrate. It consists of two ground slots and multiple T slots to achieve broadband at 1.06 GHz and 5.8 GHz with circular polarization. The proposed antenna has dimensions of 62.3 mm \times 59.7 mm with a good gain.

Compared to the above mentioned designs this work achieves integration of the Superformula geometry with dual band circular polarization performance. Further the use of CPW feed has reduced the design to a single layer. Thereby reducing cost, complexity and thickness of the design. The application of multiple slots produces high efficiency and circularly polarized bands of 0.095 or 9.5% and 0.037 or 3.7% bandwidth in the C band.

Design of the multi-ringed super-formula-based antenna

The design of the proposed antenna structure begins with a CPW-fed multi-ringed superformula-based patch antenna, utilizing a Rogers RO4003 substrate (substrate thickness $h=1.6$ mm, relative permittivity $\epsilon_r=3.55$, and loss tangent $\tan \delta=0.0027$). The antenna structure is positioned in the x-y plane, with its normal direction aligned along the z-axis. The initial antenna shape is generated using the superformula, and subsequently, two rings of equilateral triangles are incorporated step by step, as illustrated in Fig. 1. The value of $a=b=1$ to achieve mirror symmetry. The value of $m=30$ to get multiple edges and the value of $n_1=n_2=n_3=5$ to position these edges on the circumference of this design.

First, a circular patch antenna structure is designed, and the first ring of polynomials is added on the circumference and simulated as shown in Fig. 1(a). To increase the bandwidth and other parameters a second ring is added over the first one, as shown in Fig. 1(b). But now the resonant frequency shifts forward in the 8 GHz range. So, a third ring is subtracted from the patch structure, which makes the structure resonate in the desired frequency range as shown in Fig. 1 (c).

A CPW feed is used to excite the proposed antenna. The dimensions of the feed are calculated using the following formula, as explained by K.P. Ray in¹⁹.

$$f = \frac{c}{\lambda} = \frac{7.2}{L + r + p} \quad (3)$$

Where,

'L' is the height of the planar monopole antenna, 'r' is the effective radius of the equivalent cylindrical monopole antenna, and 'p' is the length of the 50Ω feed line. All the units are taken in cm.

For the purpose of designing, the monopole antenna is equated with a cylindrical monopole antenna with a large diameter whose bandwidth is proportionate to its diameter. This is done because a CPW feed is designed according to the lower band edge frequency of all usual shapes of monopole antennas. We are choosing a circularly polarized antenna as a base design; we need to equate the area to a cylindrical monopole antenna. As the total surface area of a cylinder can never equal the area of its base circle, the curved surface area is thus equated with a circular patch antenna by the following Eq.

$$2\pi rh = \pi a^2 \quad (4)$$

Where, 'r' is the radius of the cylinder, 'h' is the height of the cylinder, and 'a' is the radius of the circle of equal area. The final dimensions of the feed p are calculated by substituting the value of $L=2a$, i.e. complete diameter of the circular patch and $r=a/4$, i.e. circumference divided by 2π and $f=5.8$ GHz.

The dimension of the vertices of the equilateral triangle of each ring is optimized to get maximize bandwidth output. The length of the ground plane in a CPW-fed design can be optimized since the design formula depends on the ratio between the ground plane width and the feedline width. Therefore, the length of the ground plane and dielectric substrate was reduced by 4.5 mm on each side, making the structure more compact without negatively impacting the antenna's performance parameters.

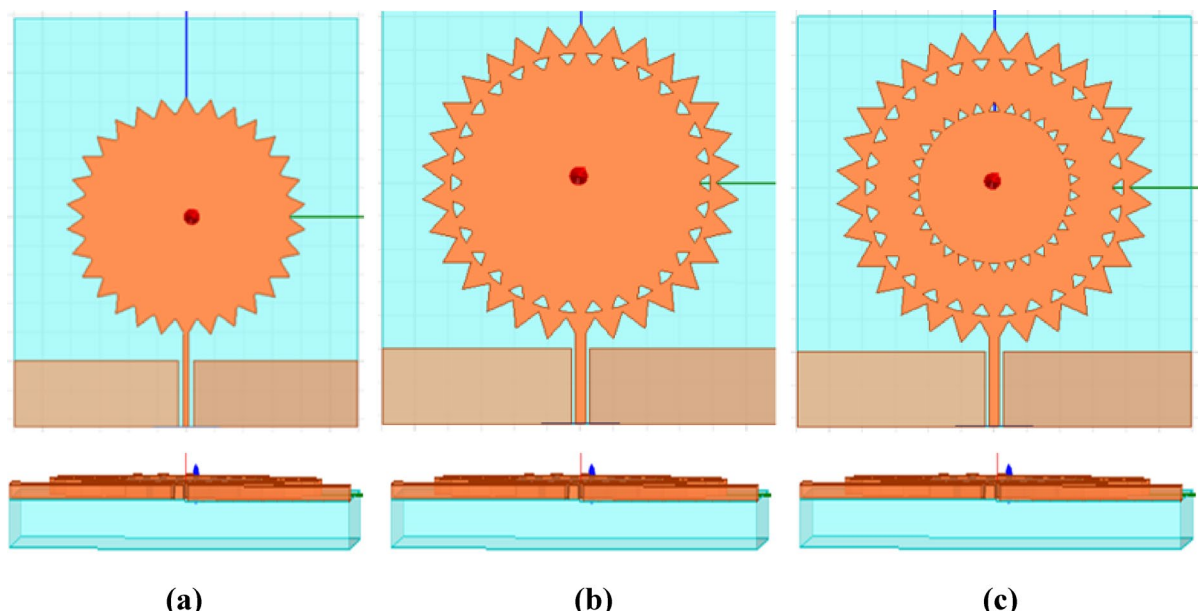


Fig. 1. Different simulated stages for super-formula-based patch antenna with their front view and side view
(a) single ringed. **(b)** Double ringed. **(c)** Triple ringed.

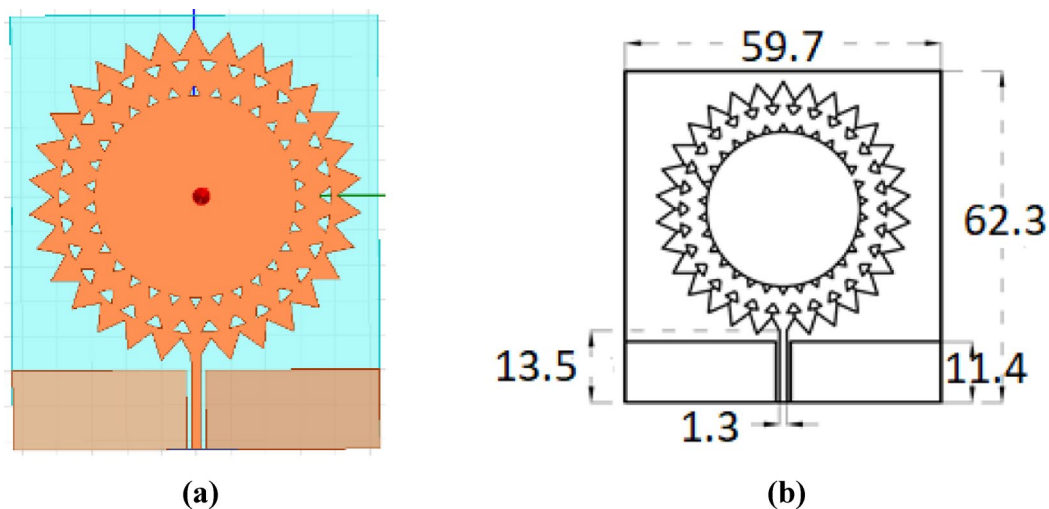


Fig. 2. (a) Simulated design of Multi-ringed Super-formula-based antenna (b) Design of Multi-ringed Super-formula-based antenna with dimensions in mm.

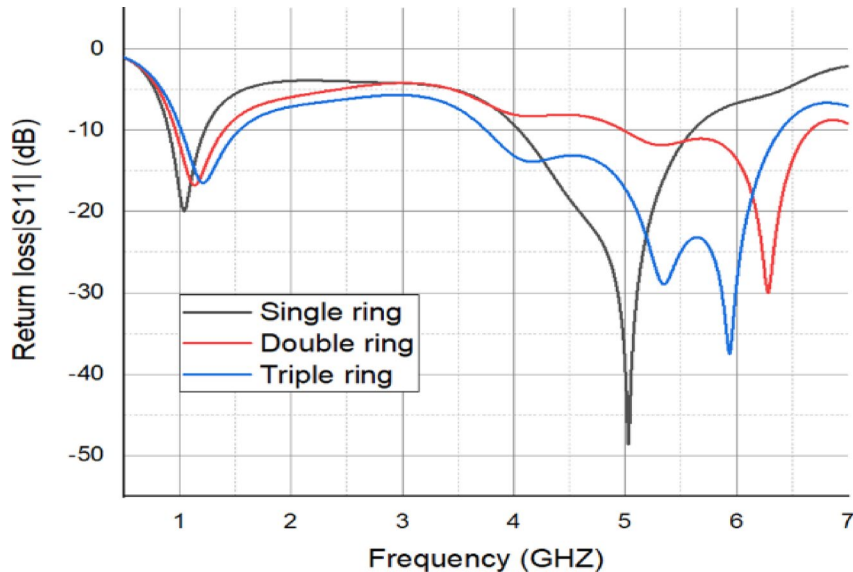


Fig. 3. The return loss graph as a function of frequency with step wise addition of rings to the antenna.

The final dimensions of the proposed structure are 59.691 mm \times 62.3 mm and the size of the vertices of the equilateral triangles is 2 mm, 3 mm, and 0.5 mm, respectively, from outside to inside, as shown in Fig. 2.

As illustrated in Fig. 3, the triple ringed patch antenna structure has a wider bandwidth than the other two designs. The simulated results indicate a dual-band broadband antenna structure with 5.94 GHz (with a bandwidth of 0.52556 GHz, or 52.56%) and 1.21 GHz (with a bandwidth of 0.41659 GHz, or 41.66%) of central frequencies.

Design of the super-formula-based antenna with circular polarization

The next step is to achieve circular polarization for the multi- ringed super-formula-based patch antenna. So, multiple slots in the ground were introduced at a 45° angle. Then a ground defect was introduced along with the slots. This improved the circular polarization bandwidth, but now the structure behaves like a single-band antenna. In the next step, multiple slots were introduced in the patch structure at various angles and optimized to improve the parameters.

It is observed that by introducing multiple T slots at 45°, -135°, and 135° each, the optimum result is obtained. This also leads to the removal of the deepest ring, as shown in Figs. 4 and 5. An introduction of an 'T' slot at 90° on the top of the patch improves the gain parameter. The dimensions of the ground slot and patch slots are shown in Table 1.

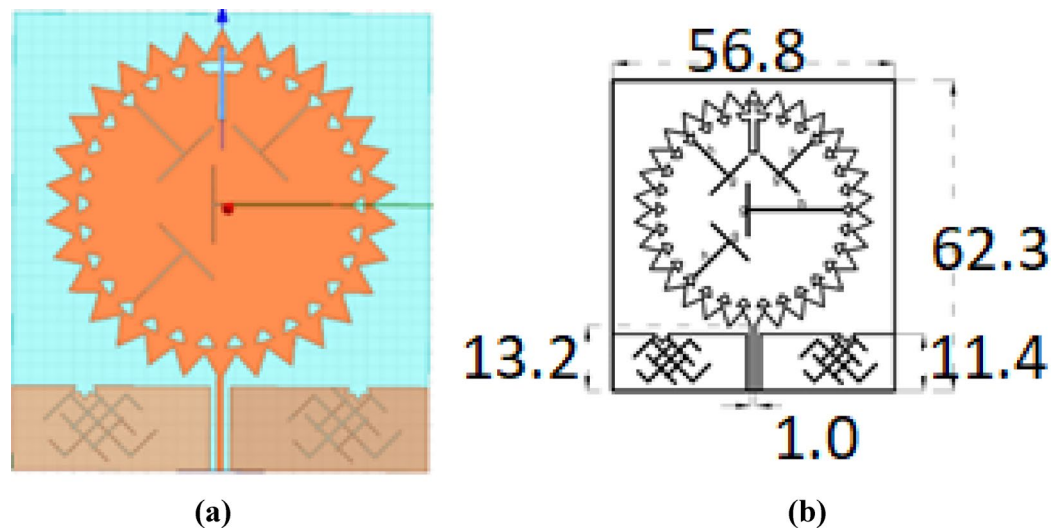


Fig. 4. (a) Simulated design of the Super-formula-based antenna with multiple T slots and ground alterations (b) Design of the Super-formula-based antenna multiple T slots and ground alterations with dimensions in mm.

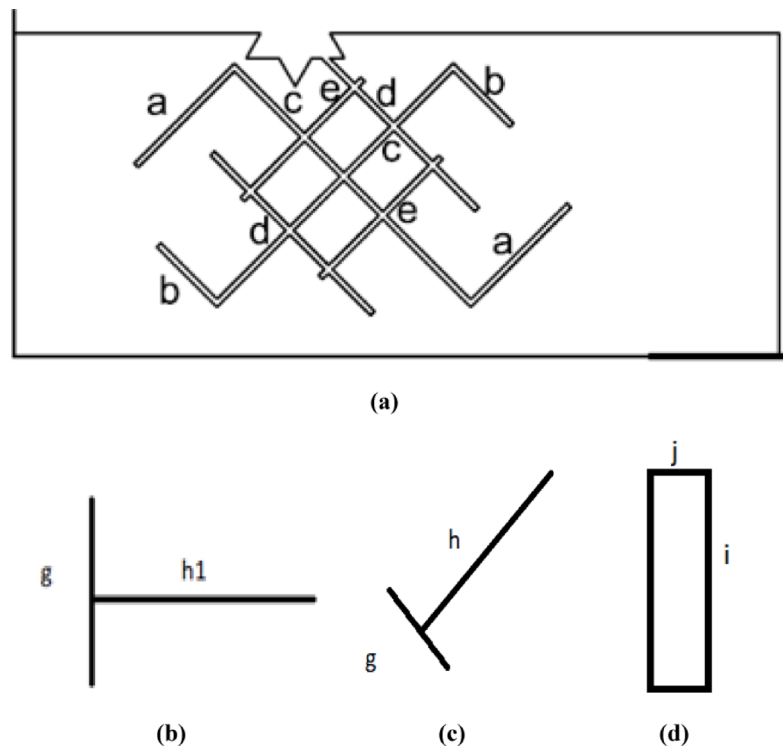
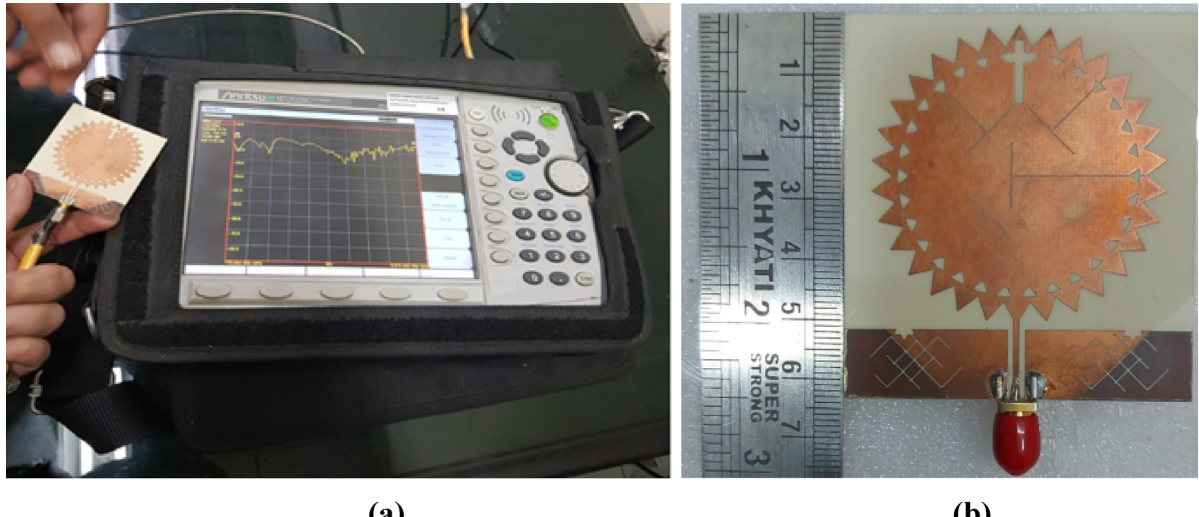
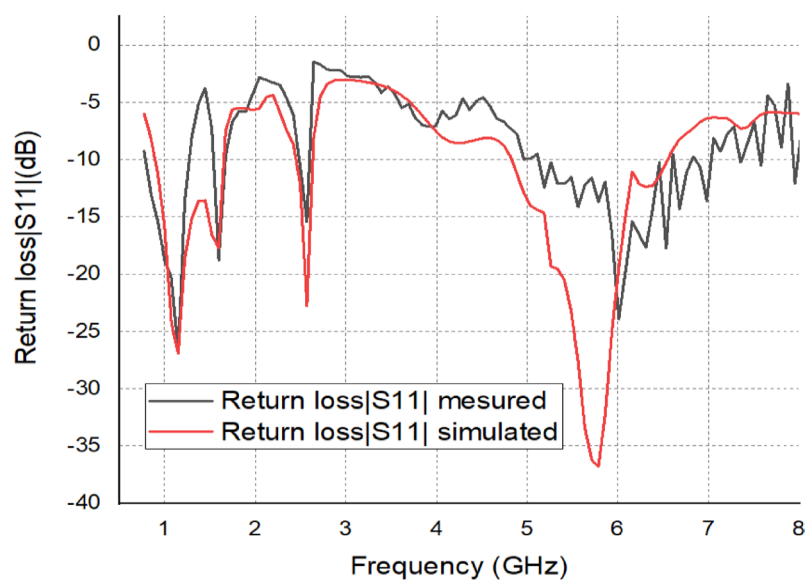


Fig. 5. Design of the (a) ground plane of the antenna (b) central T slot (c) tilted T slot (d) rectangular top slot of the antenna.

Result of the super-formula-based antenna with multiple T slot and ground modification

The proposed antenna is fabricated on a Rogers RO4003 substrate (substrate thickness $h = 1.6$ mm, $\epsilon_r = 3.55$, $\tan \delta = 0.0027$) as shown in Fig. 6 and was measured at CARE labs at IIT Delhi. The measured and simulated results of the return loss versus frequency are shown in Fig. 7, which are found in good agreement with each other. The antenna now behaves as a multi-band broad band antenna with a central frequency of 1.06 GHz (with the bandwidth of 0.670441 GHz or 67.04%), 5.822 GHz (with the bandwidth of 0.29479 GHz or 29.48%), and 2.562 GHz (with bandwidth of 0.0591 GHz or 5.9%).

Measurement of ground slot		Measurement of patch slot	
Section	Dimension in mm	Section	Dimension in mm
a	5	h1	21
b	3	g	10
c	12	h	11.5
d	9	i	10
e	6	j	1.5

Table 1. Measurement of ground slot and patch slot.**Fig. 6.** (a) Picture of the antenna with VNA at the time of antenna testing of Multi- ringed Super-formula-based antenna. (b) Picture of the Multi- ringed Super-formula-based antenna.**Fig. 7.** The return loss graph as a function of frequency for multi- ringed super-formula-based antenna.

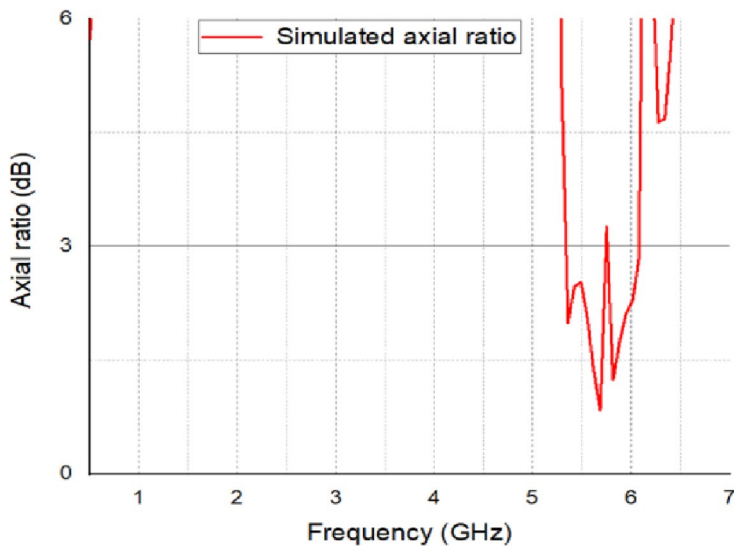


Fig. 8. The axial ratio plot of the Multi- ringed Super-formula-based antenna.

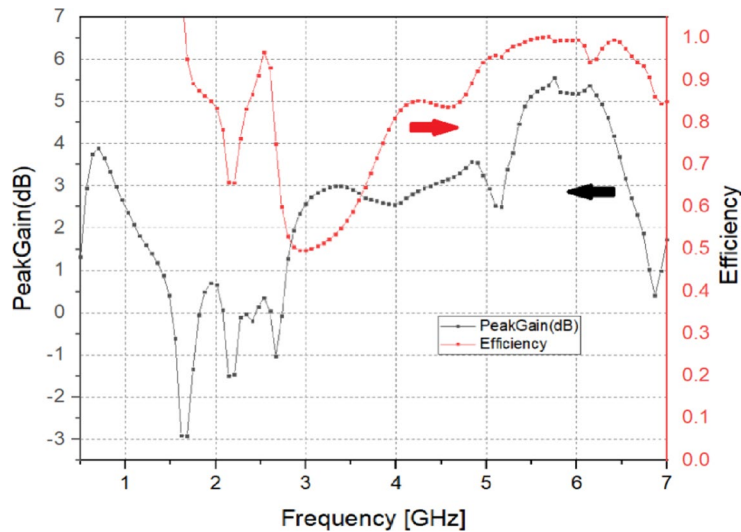


Fig. 9. The gain plot and efficiency plot of the Multi- ringed Super-formula-based antenna.

After inserting T slots in patch and other slots in ground the antenna behaves as a circularly polarized antenna in the C band with bandwidth from 5.31 to 5.75 GHz or 7% and 5.75–6.1 GHz or 11% as shown in Fig. 8.

The peak gain and the compound total efficiency are plotted in Fig. 9. The peak gain of the antenna at 5.82 GHz is 5.2 dB as shown in Fig. 9. It is found that at 5.82 GHz the efficiency is 98% which corresponds with the gain. The measured 2-D co polar and cross polar radiation patterns in elevation and azimuth planes at 5.82 GHz frequency is shown in Fig. 10 (a) and (b). It is observed that the co-polar radiation pattern is in mushroom shape with the major power radiated in the forward direction and the cross-polar radiation pattern nearly omnidirectional in nature and significantly resembles with monopole antenna. In elevation plane; the co-polar patterns at all frequencies are higher than cross polar patterns.

The surface current distribution of the antenna at 5.82 GHz is shown in Fig. 11. It is observed that the CPW feed line carries a significant amount of current along the edges of the super-formula-based structure, which is then directed towards the center through the T-shaped slots. At these locations, the electric field is generated. On the ground plane, the current is primarily concentrated along the edges near the feed and around the ground slots, where strong electric fields are also produced. These regions contribute to the generation of electric field components E_x and E_y along the x-axis and y-axis, respectively. When E_x and E_y have equal magnitudes and a 90° phase difference, the antenna achieves circular polarization (CP). Furthermore, the surface current vectors rotate in a clockwise direction, indicating that the antenna operates in right-hand circular polarization (RHCP) mode. The surface current distribution is analyzed at various phase angles of 0°, 90°, 180°, and 270°, as illustrated in Fig. 11.

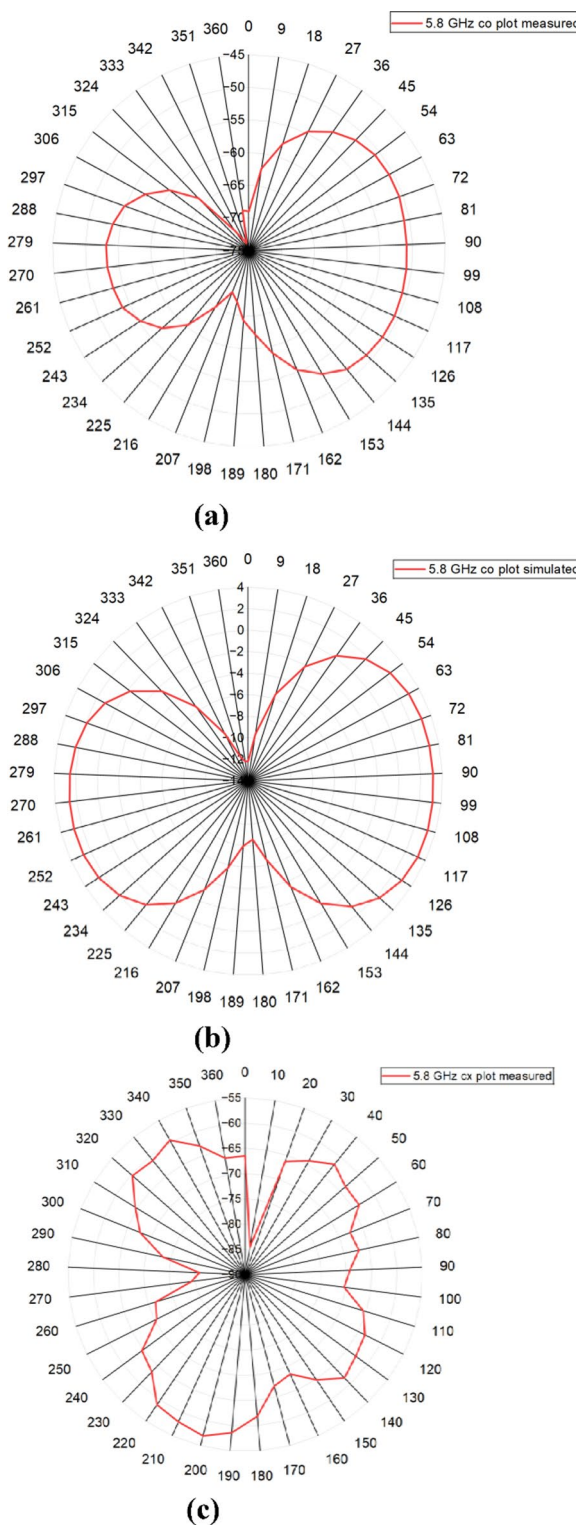
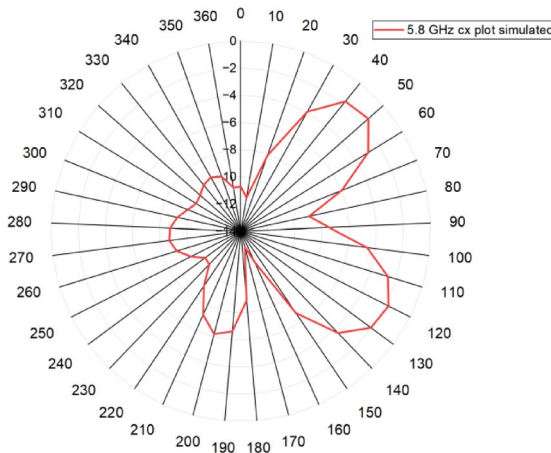


Fig. 10. The radiation pattern for the Circularly polarized Multi- ringed Super-formula-based antenna at 5.82 GHz **(a)** Measured Co-polarization, **(b)** Simulated Co-polarization, **(c)** Measured Cross polarization, **(d)** Simulated Cross- polarization.



(d)

Fig. 10. (continued)

Comparison of antenna dimensions, bandwidth, polarization and gain of the proposed antenna with other reported super-formula-based antennas is shown in Table 2. The proposed antenna is capable of achieving lower dimensions and higher gain in the C band.

Conclusion

A multi frequency broadband circularly polarized patch antenna based on Gielis's super-formula is presented in this paper. By inserting multiple T slots at a gap of 45° each and ground adjustments circular polarization is obtained. The measured peak gain and corresponding total radiation efficiency of the antenna across all operating bands are summarized as follows: 3.1 dB and 71% at 1.06 GHz, 2.4 dB and 68% at 2.56 GHz, and 5.2 dB and 98% at 5.82 GHz. These results are consistent with the simulated trends shown in Fig. 9. The high efficiency in the C-band can be attributed to the effective excitation of orthogonal modes and reduced substrate and conductor losses, while slightly lower efficiencies at the lower bands arise from the electrically smaller aperture and partial surface-wave coupling. Overall, the measured gain values confirm that the antenna maintains stable radiation performance across its multiband operation. The proposed antenna now resonates in the C band with circularly polarized bands of 0.095 or 9.5% and 0.037 or 3.7% bandwidth. The other advantages of this design are reduction in size, improvement in peak gain and peak directivity as compared to a normal patch antenna. A comparison of the various antenna results and parameters is given in Table 3.

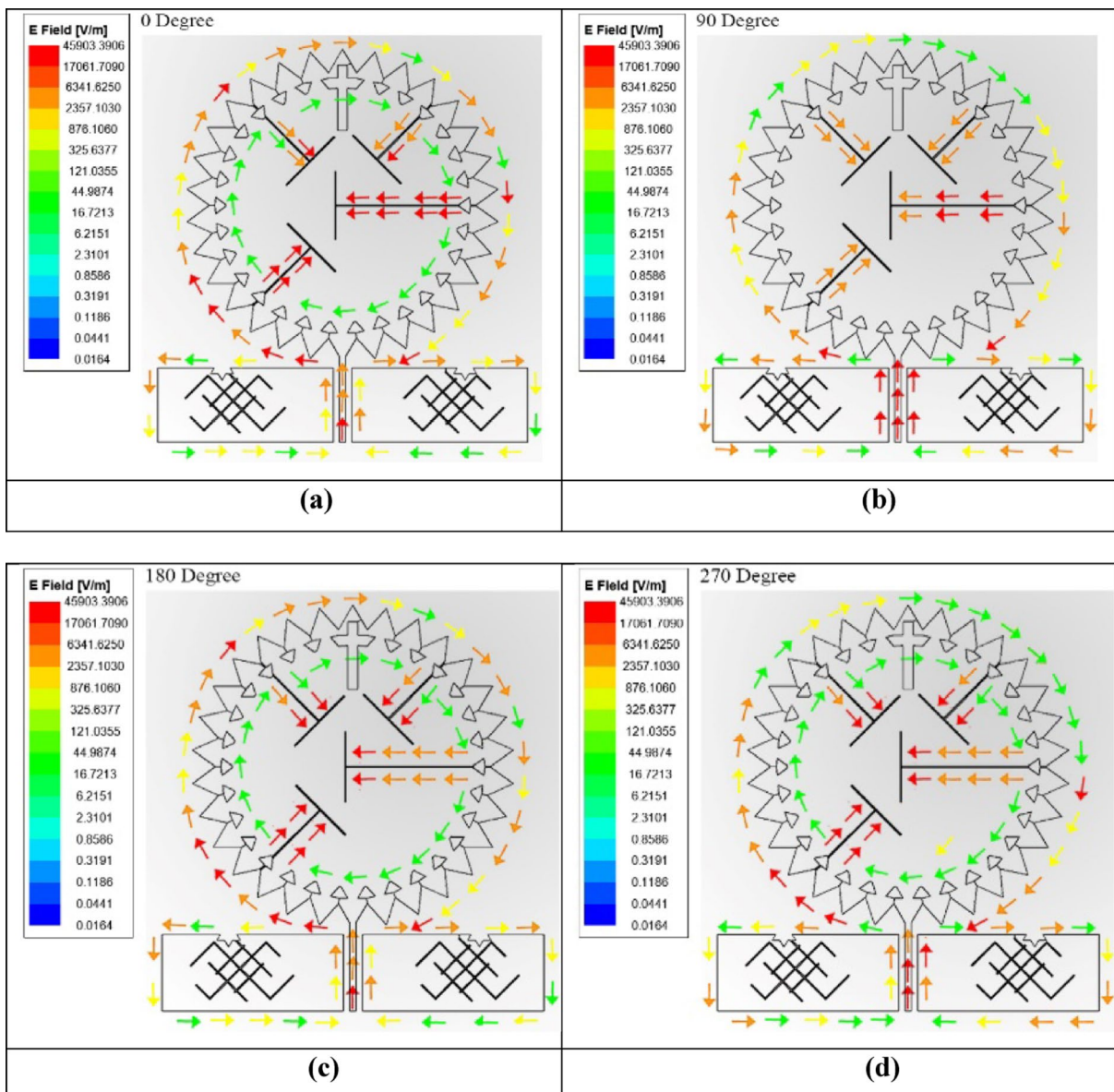


Fig. 11. The surface current distribution at 5.82 GHz frequency at various phase angles of (a) 0°, (b) 90°, (c) 180° and (d) 270°.

S.	References	Dimension (mm)	Bandwidth (GHz)	Polarization	Peak Gain (dB)
1	¹¹ /2017	52 × 35	3.1–12	Linear	5
2	¹² /2018	40 × 50	2.398–2.511	Circular	3.9
3	¹³ /2018	80 × 80	2.5–9	Linear	5
4	¹⁶ /2017	56 × 55	1.5–1.8, 2.2–2.6, 3.3–3.6, 4.8 and 5.3–6	Circular	3
	¹⁷ /2017	80 × 80	3.2–3.9 and 4.9–5.6	Circular	4
5	¹⁸ /2019	62 × 43	2.33–2.44	Linear	3.01
6	¹⁵ /2024	120 × 105	2.14–2.57 and 3.78–4.52	Circular	4.87
7	Proposed antenna	59.69 × 60.41	0.88–1.56, 2.46–2.60 and 4.87–6.49.	Circular	5.2

Table 2. Parameters for different antennas.

S.	Type of antenna	Resonant frequency (GHz)	Bandwidth (GHz)	Peak gain (dBm)	Peak directivity (dBm)
1	Multi- ring Super-formula-based antenna	5.93 1.23	0.52, 0.41	35, 33	29, 11
2	The Super-formula-based antenna with T slot and ground modification	5.86, 1.14, 2.54	0.29 0.67 0.05	35.4, 34.4, 30.1	35.4, 29.9, 30.2

Table 3. Table of parameters for different antennas.

Data availability

The data generated during this study are included within this article.

Received: 21 July 2025; Accepted: 29 December 2025

Published online: 20 January 2026

References

1. Moharana, M. & Dwivedy, B. Circularly polarized planar antennas with enhanced characteristics for contemporary wireless communication use cases: a review. *IEEE Access*. **12**, 134594–134613 (2024).
2. Sun, X. Y. et al. Ultrawideband circularly polarized halved-type Vivaldi antenna with symmetrical radiation pattern. *IEEE Antennas. Wirel. Propag. Lett.* **23** (2), 633–637 (2024).
3. A. Rahman, A. N. A review of circularly polarized dielectric resonator antennas: recent developments and applications. *Micromachines* **13** (12), 1–33 (2022). Special Issue Feature Papers of Micromachines in Engineering and Technology.
4. Motevasselian, A., Ellegard, A. & Jonsson, B. L. G. A helix excited circularly polarized Hollow cylindrical dielectric resonator antenna. *IEEE Antennas. Wirel. Propag. Lett.* **12**, 535–538 (2013).
5. Sahal, M., Yadav, D., Bhatnagar, D. & Tiwari, M. A modified-square slot antenna with circular polarization characteristics for military band applications. *Electronics/Elektronika* **26**, 46–52 (2022).
6. Omar, A. et al. Compact design of UWB CPW-fed-patch antenna using the superformula, 2016 5th International Conference on Electronic Devices, Systems and Applications (ICEDSA), 1–4, (2016).
7. Gielis, J. A generic geometric transformation that unifies a wide range of natural and abstract shapes. *Am. J. Bot.* **90**(3):333–338, (2003).
8. Omar, A. A., Naser, S., Hussein, M. I., Dib, N. I. & Rashad, M. W. Superformula-based compact UWB CPW-fed-patch antenna with and without dual frequency notches. *Appl. Comput. Electromagn. Soc. J. (ACES)*. **32**, 979–986 (2017).
9. Mao, C., Khalily, M., Tafazolli, R. & Kishk, A. Wideband dual circularly polarized helical antenna array for satellite applications. *IEEE Antennas. Wirel. Propag. Lett.* **23**, 9, 2758–2762 (2024).
10. Chen, R. S. et al. Bandwidth-enhanced circularly polarized slot antenna and array under two pairs of degenerate modes in a single resonant cavity. *IEEE Antennas. Wirel. Propag. Lett.* **22** (2), 288–292 (2023).
11. Naser, S. & Dib, N. Design and analysis of super-formula-based UWB monopole antenna and its MIMO configuration. *Wireless Pers. Commun.* **94**(4):25–28, (2017).
12. Poordaraee, M., Oraizi, H., Khajevandi, S. & Glazunov, A. A. Systematic design of a circularly polarized microstrip antenna using a shape super-formula and the characteristic mode theory, 2018 18th Mediterranean Microwave Symposium (MMS), 47–50, (2018).
13. Bhaskar, V. S., Tan, E. L., Holden Li, K. H. & Tse, M. S. Broadband CPW-fed Slot Antenna Using Superformula, 2018 IEEE International Symposium on Antennas and Propagation & USNC/URSI National Radio Science Meeting, 1277–1278, (2018).
14. Wei, K. et al. A dual-band rotational feed circularly polarized Rfid reader antenna array with stable gain. *IEEE Antennas. Wirel. Propag. Lett.* **24** (7), 1620–1624 (2025).
15. An, N. & Zhang, Y. Dual-band dual-sense circularly polarized antenna utilizing a radiating slot antenna as feeding structure. *IEEE Antennas. Wirel. Propag. Lett.* **23** (4), 1321–1325 (2024).
16. Fathima, N., Nayana, K. S., Ali, T. & Biradar, R. C. A miniaturized slotted ground fractal Koch multiband antenna for wireless applications, 2017 2nd IEEE International Conference on Recent Trends in Electronics, Information & Communication Technology (RTEICT), 251–255, (2017).
17. Goel, A., Kumar, S., Saxena, S. & Tiwari, R. Single layer proximity fed microstrip patch antenna for circularly polarized dual band wireless applications, 2017 6th International Conference on Reliability, Infocom Technologies and Optimization (Trends and Future Directions) (ICRITO), 496–499, (2017).
18. Ali, S. M., Jeoti, V., Saeidi, T. & Wen, W. Design of compact microstrip patch antenna for WBAN applications at ISM 2.4 ghz. *Indonesian J. Electr. Eng. Comput. Sci. (IJECS)*, **15** (3), 1509–1516. (2019).
19. Ray, K. Design aspects of printed monopole antennas for ultra-wide band applications. *Int. J. Antennas Propag.* 1–4, (2008).

Acknowledgements

The authors would like to thank the entire team of “Centre of Applied Research in Electronics (CARE), IIT Delhi”, for their support in the testing of the antenna. The Centre for Applied Research in Electronics (CARE) at IIT Delhi uses a VNA with an anechoic chamber for antenna testing, with specific details available for different set-ups. The measurement setup typically includes an anechoic chamber with an automatic platform, a VNAs (e.g., up to 20–67 GHz), and SMA or N-type connectors depending on the equipment. Specific details on fabrication tolerance are not publicly available in the provided search results. Fabrication tolerance, Specific fabrication tolerance values are not listed in the provided search results. Measurement setup-Anechoic Chamber: An anechoic chamber with an automatic platform controller is used for antenna testing and characterization. Vector Network Analyzer (VNA): VNAs with a frequency range of 100 MHz to 6 GHz and another up to 20 GHz are available for measuring port performance (like S-parameters and VSWR). A separate VNA up to 67 GHz is used for dielectric constant measurements. Calibration: A calibration kit is used with the VNA. The method for calibration (e.g., TRL, SOLT) is not specified. Connector Type: SMA (M) connectors and corresponding cables are used for the 100 MHz to 6 GHz VNA setup. If the VNA ports are N-type, N-SMA adapters are required, which are included in the offer. Other Equipment: The lab also utilizes digital signal analyzers (up to 25 GHz) and simulation tools such as Ansoft HFSS, Agilent ADS, and CST Microwave Studio.

Author contributions

Kanika Joshi: Write manuscript original draft, Validation, Software, Methodology, Formal Analysis, Conceptualization. Gaurav Kumar Soni: Review and editing the manuscript, Software, Methodology, Formal Analysis. Dinesh Yadav: Review and editing the manuscript, Conceptualization, Validation, Supervision, Resources.

Funding

Open access funding provided by Manipal University Jaipur.

Declarations

Competing interests

The authors declare no competing interests.

Additional information

Correspondence and requests for materials should be addressed to D.Y.

Reprints and permissions information is available at www.nature.com/reprints.

Publisher's note Springer Nature remains neutral with regard to jurisdictional claims in published maps and institutional affiliations.

Open Access This article is licensed under a Creative Commons Attribution-NonCommercial-NoDerivatives 4.0 International License, which permits any non-commercial use, sharing, distribution and reproduction in any medium or format, as long as you give appropriate credit to the original author(s) and the source, provide a link to the Creative Commons licence, and indicate if you modified the licensed material. You do not have permission under this licence to share adapted material derived from this article or parts of it. The images or other third party material in this article are included in the article's Creative Commons licence, unless indicated otherwise in a credit line to the material. If material is not included in the article's Creative Commons licence and your intended use is not permitted by statutory regulation or exceeds the permitted use, you will need to obtain permission directly from the copyright holder. To view a copy of this licence, visit <http://creativecommons.org/licenses/by-nc-nd/4.0/>.

© The Author(s) 2026